A New RadMon Version for the LHC and its Injection Lines

G. Spiezia, P. Peronnard, A. Masi, M. Brugger, M. Brucoli, S. Danzeca, R. Garcia Alia, R. Losito, J. Mekki, P. Oser, R. Gaillard, *Senior Member, IEEE*, and L. Dusseau

***Abstract*—A system to monitor the radiation levels is required in the Large Hadron Collider (LHC) and its injection lines in order to quantify the radiation effects on electronics. Thus, the RadMons were installed in critical areas where equipment is or will be placed. The first years of operation, successive test campaigns and new requirements, raised the need for a new design of the monitor. The architecture of the new RadMon, the radiation reliability and the design strategy adopted for the sensors, used for monitoring the mixed radiation field of the LHC accelerator, are described highlighting the achieved improvements in terms of radiation robustness and measurement accuracy of a device which is of interest for many other research institutes.**

***Index Terms*—Displacement damage, dosimetry, particle accelerators, single event effects, total ionizing dose.**

I. Introduction

A LARGE amount of equipment, mostly based on Commercial Off The Shelf (COTS) components, is installed in the Large Hadron Collider (LHC) tunnel and/or its adjacent services galleries, and thus exposed to a radiation field composed of different particles with energies from a few meV (thermal neutrons) up to the GeV range [1], [2]. For the ultimate LHC conditions, the Radiation To Electronics (R2E) project aims at having less than one radiation failure per week for all types of equipment installed in the accelerator and critical for the operation of the accelerator. The accurate monitor of the radiation levels is a fundamental ingredient to achieve this requirement in order to better study equipment failures or long-term degradations. Monitoring systems for accelerators, such as beam loss or beam position monitors, are conceived and designed to provide data for beam steering and beam loss detection, with limited performance for the measurement of the radiation field and quantities related to damage to electronics. Therefore, the LHC tunnel and its adjacent shielded areas were equipped with a radiation monitoring system, the so-called RadMon system [3]. The monitoring of the radiation levels permits to anticipate possible device degradation and identify instantaneous failures of electronic equipment as caused by radiations. The RadMons are also used to verify the shielding efficiency and benchmark FLUKA Monte-Carlo calculations, used to predict present and future radiation levels for the LHC locations. Those measurements are also needed by other particle accelerators and satellites' builders when COTS devices are mainly used. Moreover, the RadMon is exploited to monitor the radiation levels in the CERN test facilities where the peculiar LHC mixed radiation field is reproduced for radiation test and quality assurance purposes [4]. With 340 installed units, the RadMon system provided data on the Total Ionizing Dose (TID), the 1 MeV neutron equivalent fluence (Φ_{eq}) and the High Energy Hadron (HEH) fluence (> 20 MeV), quantities used to refer to the radiation damage to electronics caused by the Ionizing Energy Loss (IEL), Displacement Damage (DD), and Single Event Effects (SEE), respectively. For the latter, the thermal neutron fluence is also to be measured since thermal neutrons can cause SEEs in components containing Boron (^{10}B). Obsolescence of several components used for the first generation of RadMon, hereafter referred as RadMonV5, feedback from the on-field usage of the monitor in the first period of LHC operation (2010-2012), and, especially, new monitoring requirements lead to launch a new design of the RadMon, hereafter RadMonV6, which aims at resolving issues and limitations experienced with the previous version to achieve the requirements targets defined in Section II in a defined period of 4 years. Radiation hardness was improved by carefully choosing components and performing radiation tests with protons, ^{60}Co sources, and 1 MeV neutrons, first at single components level and later on the entire RadMon prototype. The new FPGA-based design permits remote control of the main settings and offers a modular architecture for an easy exchange of the sensors. The RadMon detector provides measurement of the TID by means of RadFETs, DD by means of p-i-n diodes, and HEH fluence by counting Single Events Upsets (SEU) of SRAM memories. The acquisition chain and the analog circuitry of the sensors was changed to profit from the gained knowledge during the calibration campaigns in standard European facilities as well as in CERN experimental areas [4]–[10]. The stored and the new bought batches of RadFETs have been calibrated in three different ^{60}Co facilities up to 1 Mrad(Si), and with protons at different energies (60-230 MeV). The batches of p-i-n diodes have been irradiated at a nuclear reactor up to an 1 MeV neutron equivalent fluence of $5 \cdot 10^{14}$ cm^{-2}. The SRAMs used on the previous RadMon version and the ones foreseen for the new monitor, have been calibrated with neutrons (thermal, 5, 8 and 14 MeV) and protons (30-480 MeV). Finally, all calibrations

Manuscript received July 11, 2014; revised September 23, 2014; accepted October 23, 2014. Date of publication November 06, 2014; date of current version December 11, 2014.

G. Spiezia, P. Peronnard, A. Masi, M. Brugger, M. Brucoli, S. Danzeca, R. Garcia Alia, R. Losito, J. Mekki, and P. Oser are with European Organization for Nuclear Research (CERN), CH-1211, Geneva 23 Switzerland.

S. Danzeca, R. Garcia Alia, and L. Dusseau are with the IES, F-34000 Montpellier, France.

R. Gaillard is a Consultant, Saint-Arnoult, Yvelines, France.

Color versions of one or more of the figures in this paper are available online at http://ieeexplore.ieee.org.

Digital Object Identifier 10.1109/TNS.2014.2365046

will be applied in the CERN test facilities, notably the one for mixed-radiation fields where the respective RadMon response can be compared with the expected radiation field response.

Monitors similar to the RadMon are also used in the space community [11], [12] and an adapted version of the RadMon is currently under study to be used in a future cubeSat in connection with a dedicated latch-up experiment. Many particle accelerators use COTS electronics and wish to on-line measure the evolution of the radiation levels to understand the degradation of the equipment and identify instantaneous failures. The simultaneous measurements of the three quantities to determine damage to electronics help to bench mark numerical calculations and understand complex field. After recalling the peculiarities of the LHC radiation fields and the requirements for the new RadMon, the adopted design, and the radiation assurance plan are described. Then, the strategy to exploit each of the three modes of radiation damage, TID, DD, and SEE, is explained by presenting a summary of the most recent calibration results.

II. Environment and Design Requirements

The variety of radiation source terms present in a particle accelerator results in a unique radiation field composed of different particles at various energies which will provoke the three different types of radiation damage. HEH radiation levels range from a few 10^7 cm^{-2} (protected, shielded areas) to 10^{12} cm^{-2} (tunnel areas) per year, corresponding to an annual TID range of 1 rad-100 krad(Si) [1]. The new RadMon system will also be deployed in the CERN injection lines, several smaller particle accelerators which feed the main LHC ring, where radiation levels up to 100-1000 krad (Si) (with hadron fluence to 10^{13} cm^{-2}) are to be expected at the location of the electronic equipment. Electronic systems containing only COTS components, installed in the shielded areas, can already fail at hadron fluences as low as 10^7 cm^{-2}; damage to COTS components, used in custom designed boards, is not negligible starting from doses of 1-10 krad (Si). Therefore, the RadMon must be able to measure radiation levels induced by a hadron fluence ranging from a few 10^7 to 10^{13} cm^{-2}, providing an evaluation of the TID, the hadron fluence, and 1 MeV neutron equivalent (Φ_{eq}). Modelling the radiation field composition by means of the FLUKA Monte-Carlo calculations, we can define the range of those quantities and the equivalence among them. The individual measurement (of dose/fluence) accuracy of the monitor aims at being in the order of 20% in calibrated fields (not exceeding a factor 2 in complex and unknown radiation environments) while the required resolution of the RadMon has to be 10% of the minimum measurement value (Table I). The specified accuracy is larger than the resolution since it takes into account the composition of the several uncertainty terms, not only related to the electronics, but also to the sensors, the calibration, and the radiation environment composition. The FLUKA calculations can provide the ratio among the three radiation damage quantities, thus to a certain extent it is not required to measure all the three quantities with the most demanding resolution over the entire measurement range, especially as those ratios can be also obtained by measurements at lower radiation levels.

For what concerns the main RadMon life time, the TID limit of the electronic components must be improved by a factor of 3 with respect to the existing RadMonV5, which was 8 krad (Si), in order to decrease the number of maintenance interventions and allow for the deployment of the system also in the CERN injector chain where high radiation levels are reached in various locations. Data acquisition, as well as the eventual configuration of the sensors is to be remotely handled to reduce the number of accesses to the tunnel.

III. Design Choices for the New RadMon

Fig. 1 depicts the general architecture of the new RadMon device which is built on 4 printed circuit boards for easy maintenance and flexibility purposes: a) the PowerBoard, b) the MainBoard, c) the Sensor Board, and d) the Deported Module. The PowerBoard includes the main DC power supplies for the analogue and digital circuitries by using AC transformers and linear regulators. The MainBoard holds the control, the monitoring and bus physical interface components, hosting the heart of the system, an Actel ProAsic3 FPGA, which embeds several custom controllers in order to process data coming from the field bus and the management of the peripherals (ADCs, sensors). The Triple Modular Redundancy (TMR) mitigation technique is applied to both registers and internal RAM to keep the core radiation tolerant; it was automatically deployed by a commercial synthesis tool and verified with proton radiation tests during the prototype phase. *Synopsys Synplify* was used for the synthesis and implementation of TMR. The penalty is an increase from to 34% to 59% of used core cells. The number of Block RAMs was multiplied by 3. The RAM blocks have been triplicated in the code since *Synplify* is not able to do it automatically. Two 8-channels 16 bit ADCs are used to acquire the dosimetry sensors and other signals (images of voltages and currents) to monitor the status of the board. The SensorBoard is populated with the TID, DD, and SEU sensors and the associated reading circuitries. This board is mechanically plugged to the MainBoard via connectors to allow changing the sensor types and/or the related analogue circuitry without affecting the MainBoard. The SensorBoard can be connected via a cable to the Deported Module which can then host the TID, DD and temperature sensors without any additional circuitry required in order to measure the TID and DD effects in locations at high radiation levels where the MainBoard and the sensor circuitry cannot work properly.

Concerning the SRAM management, the new RadMon allows the user to use two SRAM banks and control the voltage supply (1.8 V, 2.5 V, 3 V, 3.3 V, 5 V) and the initial pattern of each bank. The voltage is set remotely through the field bus. A bank is composed of four memories and this number can be extended by increasing the board area. The SEU detection algorithm in SRAM memories is straightforward. A known pattern (set remotely by the user) is written in the memory array. Then, the content of the SRAM devices is quasi continuously compared by the controller with the original pattern. In case of an observed bit error, the controller performs the following tasks: 1) the error counters for SEU and MBU are updated according to the event (single or multiple); 2) the faulty address is written back with the correct pattern.

For the reading of the RadFET and p-i-n diodes, their threshold (RadFET) and forward (p-i-n diode) voltages are

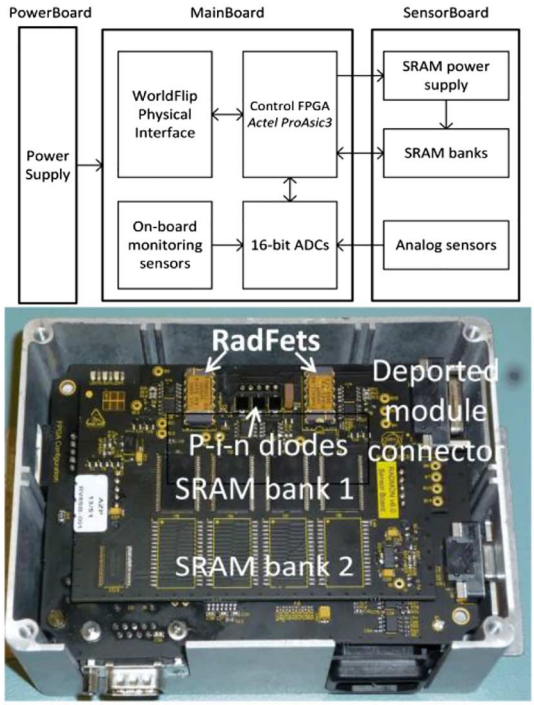

Fig. 1. General design architecture of the new RadMon (top) and a picture of the device (bottom).

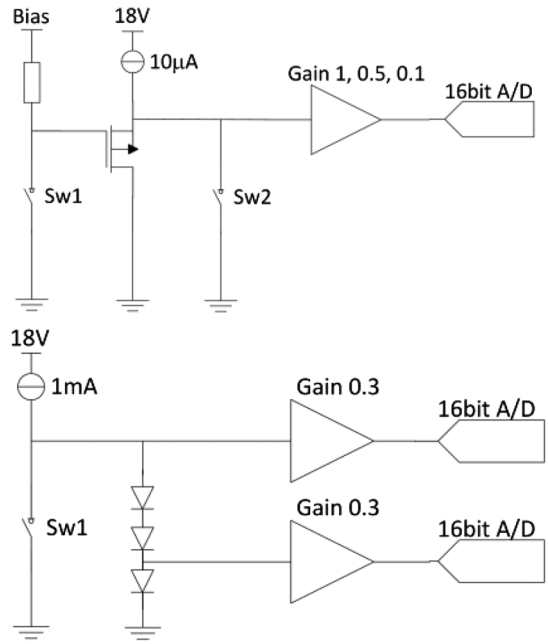

Fig. 2. Reading circuitry of the RadFETs (top) with the option of applying a bias to the gate (5 V), and p-i-n diodes (bottom).

measured by using the circuit depicted in Fig. 2. The readout protocol for these voltages is to perform a sweep measurement while the sensor is supplied with a constant current source. The sweep time, 100 ms by default and adjustable remotely by the user, is chosen according to the response time of the sensor. The measurement period of 2 s can also be remotely configured by the user (a mask is applied to the switch register). Once the measurement is done, the sensor pins are normally shorted to ground by means of MOS switches. When the reading is not enabled, a fixed bias voltage of 5 V can be applied to the gate of the RadFETs in order to increase its sensitivity as will be detailed later in the paper. The voltage is read by the ADC and a gain can be applied to exploit the full range of the instrument. The gain can be set to 1, 0.5, and 0.1 for the RadFETs while it has been fixed to 0.3 for the pin diodes. The software architecture to read out the data from the RadMon via the field bus is described in [14].

IV. Radiation Assurance

The new RadMon was designed to work up to a TID of at least 25-30 krad (Si). The main components, such as the voltage regulators, the current sources, the signal amplifiers, the ADC, and the FPGA were carefully selected and tested under radiation with 230 MeV protons (up to $6 - 8 \cdot 10^{11}$ p/cm^2) and 1 MeV neutrons (up to $4 \cdot 10^{12}$ n/cm^2) [13] to verify their robustness against the TID, soft and hard SEEs, and DD effects. A further test was done at low dose rate (400 rad/h) with a ^{60}Co source reaching a TID of 50 krad (Si). Up to a TID of 50 krad (Si) and 1 MeV equivalent neutron fluence of $4 \cdot 10^{12}$ n/cm^2, the chosen analogue components show a variation of their main parameters which is given in Table II; furthermore the effect of that variation was propagated at system level to verify that it does not affect the accuracy of the reading sensors circuitries. The drift of the output of the voltage regulators feeding the SRAM memories will not affect the memory sensitivity; the output of the current source shows a variation of a few percent which does not modify the radiation response of the RadFETs, nor of the p-i-n diodes. The FPGA works correctly up to a TID of 35-40 krad (Si). The limit of 25 krad (Si) is actually imposed by the ADC which stops working correctly; in Fig. 3, the total current consumption of the analogue and digital voltage supplies for one ADC is extrapolated from the measurements. The ADC exhibits a continuous current consumption increase, starting from 15 krad (Si). In those conditions, the transformers cannot source the current demanded by other regulators and the correct functioning is lost. Considering that the RadMon has two ADCs, the current budget for one ADC has been fixed at 500 mA. The power board can supply two ADCs up to 25 krad(Si).

As mentioned before, to measure radiation levels in locations where the TID values are above the design dose of 25 krad(Si), the sensors for TID and DD will be mounted on the Deported Board, populated with passive components only, and connected to the Sensor Board with a shielded cable which does not degrade the sensors' signal quality. Moreover, throughout the detector lifetime, the voltages, currents and ambient temperature are continuously monitored to automatically verify if the hardware is working within its specifications.

V. Strategy for the Sensor Choice and Reading

The new design improves the accuracy, the resolution and the measurement ranges of the previous version, to meet the requirements of Table I. Given the types of equipment installed in the LHC and on the basis of the experience of the first years of operation, we expect to have soft and destructive single events at a hadron fluence of 10^7 and 10^8 HEH/cm^{-2} respectively,

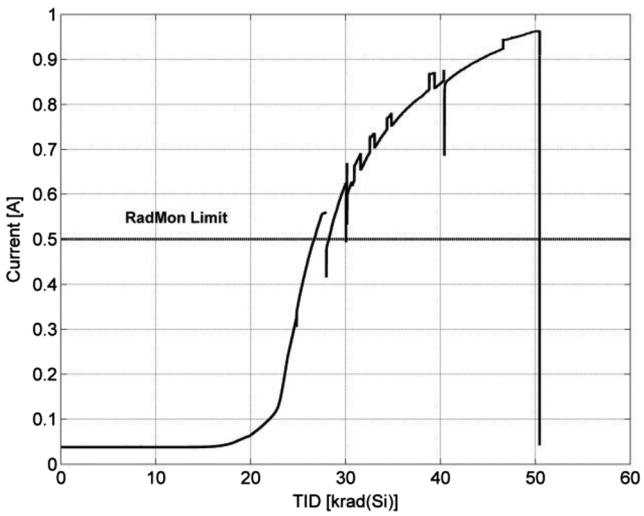

Fig. 3. Current consumption of one ADC as a function of the TID.

TABLE I
QUANTITIES RANGE WITH THE REQUIRED ACCURACY AND RESOLUTION

	Range	Resolution	Accuracy
HEH [cm^{-2}]	10^7 - 10^{13}		
TID [rad]	2 - 2·10^6	10%	x 2
1 MeV eq. [cm^{-2}]	4·10^7 - 4·10^{13}		

TABLE II
VARIATION OF THE PARAMETERS OF THE ANALOGUE COMPONENTS TO A TOTAL IONIZING DOSE OF 50 KRAD (SI)–^{60}Co SOURCE, AND 1 MEV EQUIVALENT NEUTRON FLUENCE OF $4 \cdot 10^{12}$ n/cm^2 (EXCEPT FOR THE NEGATIVE VOLTAGE REGULATOR)

Part	Max variation [%]	
	^{60}Co	1MeV neutron
OP Amp	V_{out} : 0.2	V_{out} : 0.2
Positive Voltage reg. 18 V	V_{out} : 0.4	V_{out} : 2.0
Positive Voltage reg. 5 V	V_{out}: 0.5	V_{out}: 2.0
Current source 10 µA	I_{out} : 4.9	I_{out} : 15
Current source 1 mA	I_{out} : 0.9	I_{out} : 1
Negative voltage reg. -3V	V_{out} : 0.4	V_{out} : 2% (2·10^{12})

and long term damages at a dose and 1 MeV neutron equivalent fluence higher than 1 krad(Si) and 10^{12} n/cm^{-2}, respectively. Thus, we aim at reaching the minimum required resolution for the HEH fluence (Table I) and a resolution for the TID and DD effects such to measure those two quantities in the ranges where those damages are significant (> 500rad(Si), $> 5 \cdot 10^{11}$ n/cm^{-2}).

A. Total Ionizing Dose - RadFET

The previous RadMon used three NMRC RadFets with three different oxide thicknesses, 100 nm, 400 nm and 1 μm, read in zero-bias mode to measure the TID. The thicker oxide provides the higher resolution and the lower measurement range. The use of three thicknesses aimed at achieving three different resolution, 100 rad (100 nm), 4 rad (400 nm), 1 rad (1 μm) to cover a TID up to 500 krad(Si). The resolution values, based on the data provided by the manufacturer and verified by means of a calibration with a ^{60}Co source, correspond to a variation of the threshold voltage of the RadFET of 2.4 mV, which is the Least Significant Bit (LSB) amplitude of the ADC employed on the RadMonV5. The use of the RadMon in a mixed radiation field and further calibration campaigns with protons and ^{60}Co source revealed some drawbacks of this strategy that are summarized after recalling the general plan that we adopt for calibrating the RadFETs. The employed strategy foresees the calibration of the sensors with a ^{60}Co source to have a reference response curve, verify the spread among samples, and evaluate the effect of other parameters like dose rate, annealing rate, temperature and gate bias. Then, the sensors are irradiated with protons to verify whether the radiation response changes with respect to the radiation source (protons and ^{60}Co) and/or depends on the energy of the incoming protons. Finally the ^{60}Co calibration curve is used to read the sensor in the representative mixed radiation field and verify the results with the FLUKA calculations.

The calibration and the analysis of the 1 μm RadFET showed that the sensors were not stable because a packaging issue increased the spread among the samples stored in the magazine for long time, and deeply affected the response curve. By applying the ^{60}Co calibration curve, on-field data showed that the 400 nm RadFET, almost systematically measured a TID value 40% lower than the one given by the 100 nm RadFET since the contribution of charged hadrons, in particular protons in the energy range below 100 MeV, can reduce the RadFET response [5]. Moreover, the 400 nm RadFET response showed a dependency on the dose rate which might indicate that this RadFET suffers the fading phenomenon [6]. Since thick oxide RadFETs can introduce further terms of uncertainty in a mixed radiation field, the new design is mainly focused on the 100 nm RadFET which gave results consistent with measurements of other detector types (e.g. ionization chambers), as well as FLUKA calculations in several LHC locations with different radiation field composition and dose rates during the first two years of LHC operation. Fig. 4(a) reports the calibration curves of the 100 nm RadFETs obtained with a ^{60}Co source at 25 and 40°C, which are the typical operating temperatures of the sensor board and deported module, and with protons at 230 MeV at a dose rate of 5 krad(Si)/h. Each curve represents the average of the response of three samples; the estimated standard deviation among samples is 4%, leading to an estimated 95% coverage interval of $\pm 8\%$. The RadFETs were tested with the gate biased to 0 and 5 V. If one takes as a reference the response curve with ^{60}Co at 25°C, the percentage difference among the tests at different temperatures and radiation sources is within 20% for both the cases of 0 and 5 V bias. The test with ^{60}Co at 25°C was also performed at different dose rates (100, 500, 5000 rad(Si)/h,) and the relative difference resulted to be only 5%. The voltage threshold at 25 and 40°C decreases of 6% and 3% after 5 days of annealing with a bias of 0 and 5 V respectively. The samples were kept

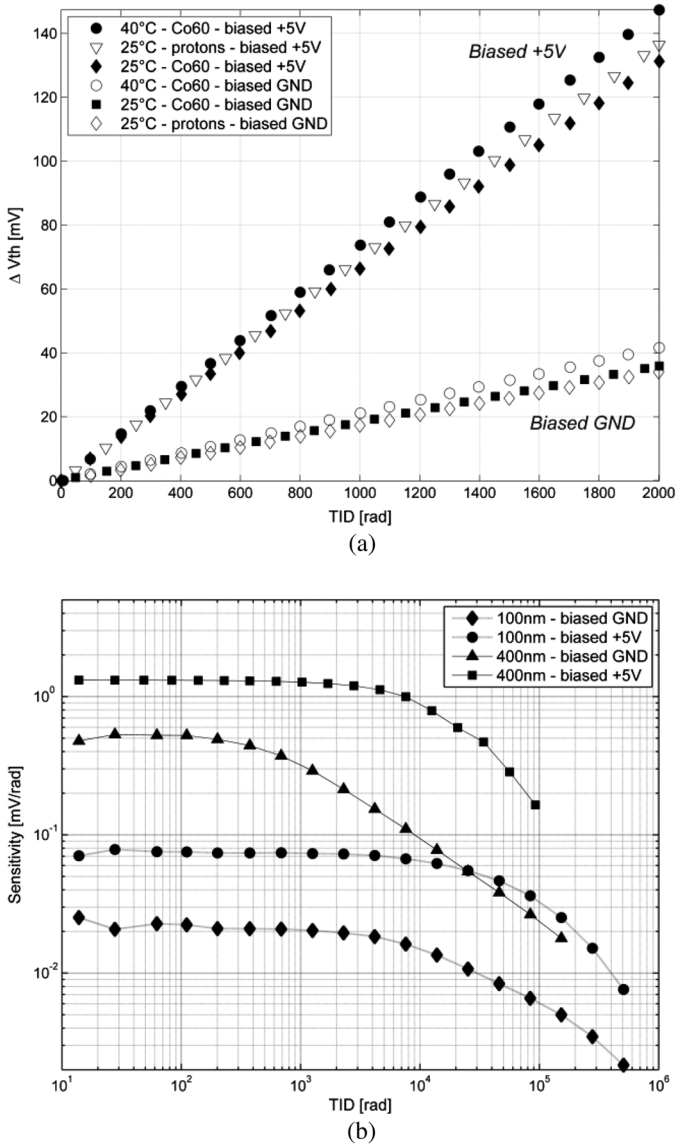

Fig. 4. (a) Average response curves for the 100 nm RADFET with gate biased at 0 V and at 5 V. This figure shows how the RADFET sensitivity is increased significantly by gate bias, and slightly by temperature variations from 25°C to 40°C. Sensitivity to TID from ^{60}Co and 230 MeV p agree within 5% at 25°C. (b) Sensitivity as a function of the dose with different gate bias for the irradiation with ^{60}Co at 40°C for the 100 nm and 400 nm RadFETs. The uncertainty of the measurement ($\pm 8\%$ and $\pm 10\%$ for the 100 and 400 nm RadFETs, respectively,) is not reported in the plot since it would be difficult to read.

TABLE III
SUMMARY OF THE EFFECTS OF EXTERNAL PARAMETERS ON THE RESPONSE CURVES OF THE 100 AND 400 NM RADFETS

Effect	100nm	400nm
Temperature	16%	-
Dose rate	5%	20%
Source	5%	-
Fading 5 days	0V (1Mrad): 6% 5V(1Mrad): 3%	0V (100krad): 15% 5V (100krad): -
Fading 2 months	0V: 10% 5V: 4%	0V: 20% 5V: -
Bias sensitivity (0-1krad(Si))	5V: 0.07 mV/rad 0V: 0.02 mV/rad	5V: 1.4 mV/rad 0V: 0.4 mV/rad

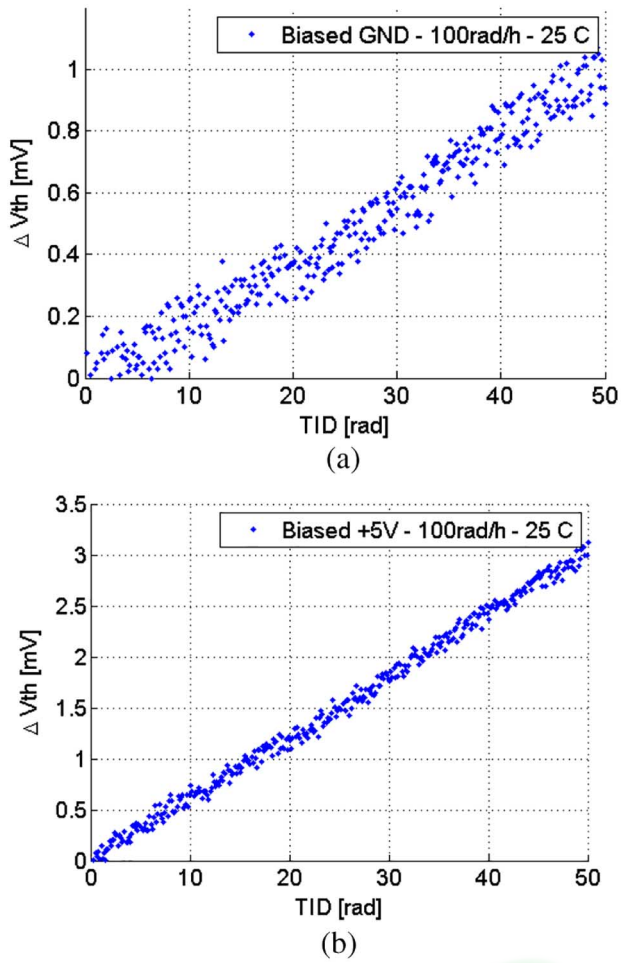

Fig. 5. RadFET response with a ^{60}Co source at 0 V (a) and 5 V bias (b).

at room temperature and measured after 2 months and the maximum voltage decrease is 10% (Table III).

Since the sensitivity of the 100 nm RadFET is only ~ 0.02 mV/rad in the 0-1 krad (Si) range, and then it decreases at higher doses, it was decided to improve the resolution of the RadMon acquisition system with a 16-bit ADC on a Full Scale Range (FSR) of ± 5V, which provides a LSB of 150 μV. Thus, considering an ADC noise of 3 LSBs, the minimum measurable TID variation is 20 rad(Si). Fig. 5(a) reports the calibration data recorded with a 7-digit multi-meter and shows that 100µV is the intrinsic noise of the sensor. The RadFET polarization circuit of the RadMon was modified with respect to the previous version to include the option of applying a bias voltage to the gate in order to improve the sensor sensitivity and thus reach the TID resolution to 6 rad(Si) (Fig. 5(b)).

Fig. 4(b), reporting the sensitivity of the 100 nm RadFET evaluated with ^{60}Co source at 40°C in the range 0-1 Mrad(Si) with 0 and 5 V bias, shows that the sensitivity is almost constant in the range 0-1krad(Si), and then decreases. The highest sensitivity is reached at low dose because the RadFET response curve is sub-linear. Since the RadFET signal can exceed 5 V, the maximum analog voltage of the RadMon has been raised to 15 V, foreseeing to apply a gain 1, 0.5 or 0.1 to the signal at the ADC inputs (Fig. 2). Thus, the new RadMon will assure a resolution of 20 rad(Si) and 6 rad(Si) in the range 0-1krad(Si)

with the 100 nm RadFET in 0 V and 5 V bias mode, respectively. The maximum measurable range is reached by the zero bias RadFET, which can measure up to 1 Mrad(Si) if mounted on the deported module.

The 400 nm RadFET from a new wafer was also investigated since it is supposed to be less dependent on the dose rate and fading effects with respect to its previous productions. The sensor was calibrated with a ^{60}Co source at 100 and 500 rad(Si)/h, and with and without bias at 5krad (Si)/h. Three samples were irradiated for each test and the average curve was evaluated together with its spread; the estimated standard deviation among samples is 5%, leading to an estimated 95% coverage interval of ±10%. The dose rate effect resulted to be 20%, which is better than what was obtained with the previous production (30%) but still worse than the 100 nm. In the range 0-1krad(Si), the sensitivity is 1.4 and 0.4 mV/rad with and without bias (Fig. 4(b)), respectively, corresponding on the new RadMon to a resolution of ~0.4 and 1 rad(Si), assuming a noise of 3 LSBs. It is noted that the sensitivity of the 400 nm RadFET without bias decreases with the dose at 1 krad(Si) since the response curve of this Radfet becomes sub-linear in the range 1-2krad(Si). The same effect appears at $\sim$ 7 krad(Si) for the 400 nm with bias. Concerning the fading effects, the 400 nm exhibited a voltage threshold decrease of 15 and 20% after 5 days and 2 months, respectively (Table III).

Unfortunately, it was not possible to evaluate the fading for the RadFET in bias mode since the measuring instrument reached its full scale during the irradiation and the threshold voltage was not measured correctly at the end of the run. Proton tests have not yet been carried out to check how the response curve of this new RadFET depends on the radiation source.

The 100 nm RadFET respects the requirements described in Section II and can be mounted on the RadMon, either on the Sensor Board or on its deported module to achieve an accuracy of 20% with a resolution of 6 rad (Si) with the bias method. The 400 nm RadFET gives a better resolution but has still a significant dependency on the dose rate and the effect of the radiation source and temperature remains to be evaluated.

Moreover, the use of a Floating Gate sensor, which could assure a resolution as low as 0.1 rad(Si) is currently under study. The same calibration plan has been applied and the results are discussed in [15]. Those sensors (the 400 nm RadFET and the Floating Gate) could eventually be considered for a future version of the RadMon.

B. HEH Fluence - SRAM

The RadMonV5 employed a $4 \times 4 -$ Mbit Toshiba SRAM TC554001AF7L. A specific method, requiring two measurements with a manual intervention on the monitor to modify the SRAM voltage, was used to measure the HEH (> 20MeV) and thermal neutron fluences with a resolution of $2 \cdot 10^6$ cm^{-2} per count [8]. The new RadMon uses an additional SRAM bank populated with $4 \times 8 -$ Mbit Cypress SRAM CY62157EV30. This memory has been chosen because it is latch-up free, has a larger size and a higher cross section to HEH fluence than the Toshiba one, is not sensitive to thermal neutrons (the thermal neutron cross section is two orders of magnitude lower than that of high energy hadrons), nor to the voltage supply, and works properly up to 30 krad (Si) [10]. Both SRAMs have been qualified with protons in the 30-230 MeV range as well as with thermal neutrons, thus allowing in the new design to use either one type or a combination of the two SRAMs. In general, the uncertainty linked to using a proton response as opposed to the real HEH one, which includes also pions, will be smaller than other sources such as that of the simulation of the radiation field, the exact location of the component or the part to part sensitivity spread. In environments with a significant proportion of pions, these normally peak at energies larger than their resonance ($\sim$ 150 MeV, [2]), therefore their contribution is very similar (or even lower) than what is expected from considering protons.

TABLE IV
SEU CROSS SECTION FOR THERMAL NEUTRONS AND 230 MEV PROTONS. THE QUOTED ERROR IS DOMINATED BY THE SPREAD AMONG SAMPLES EVALUATED AS $\pm 2 - \sigma$ STANDARD DEVIATION

	SEU Cross section (± Err) [cm^2/bit]	
	Thermal Neutrons	Protons 230 MeV
Raw data	4.4x10^{-16} (2.2)	1.9x10^{-13} (0.8)
Corrected data	4.4x10^{-16} (2.2)	3.8x10^{-14} (0.15)

The SEU cross section is reported in [8] for the TOSHIBA ($3 \cdot 10^{-14}$cm^2/bit at 5 V) and in Table IV for the CYPRESS. Chips belonging to the same lot were tested and the average of the cross section is reported for one of those lots [10]. The error is dominated by the spread among the samples of a given lot, which is by far larger than the uncertainty due to the counting statistics (3%) and the beam calibration (10%). However as each RadMon has 4 chips of the same memory, the accuracy improves in average by a factor 2.

Use of two SRAM banks allows retrieving the HEH and thermal fluence with one single measurement and without changing the voltage supply, since the Cypress memory is not sensitive to thermals. With the aim of improving the accuracy in a mixed radiation field, the SRAMs were also calibrated with neutrons at energies of 14, 8, and 5 MeV, and with 480 MeV protons at the TRIUMF facility, permitting to evaluate the cross section curve of the SRAMs from few MeV up to 480 MeV. The detailed knowledge of the radiation field in calibrated LHC test facilities is used to benchmark the calculations and study the accuracy of the monitor. These results are reported in [8].

Use of 4 CYPRESS SRAM results in a resolution of $1.5 \cdot 10^5$ cm^{-2} per count which leads to a measurement with good statistics (> 100 counts) for a fluence of $\sim 1.5 \cdot 10^7$ cm^{-2}. Fig. 6 reports the upsets of one SRAM with a cross section of $1.5 \cdot 10^{-13}$ cm^2 during 20 minutes of irradiation. The cross section of this specific chip is lower with respect to the average and gives a resolution of $8 \cdot 10^5$ cm^{-2} per count. The test has been done at an average flux of $6 \cdot 10^6$cm^{-2}s^{-1} at which a rate of $\sim$ 8 count/s is expected. It was observed that the SEU rate is not always constant and suddenly increases by a factor up to 5-8 because of error bursts [16][17]. Those error bursts were not evident during the tests with protons at a flux of $1.5 \cdot 10^8$ cm^2/s since they do not play a significant role at high flux when the SEU rate is above 100 counts/s. Conversely they compromise the accuracy of the SRAM as hadron counter at low flux since

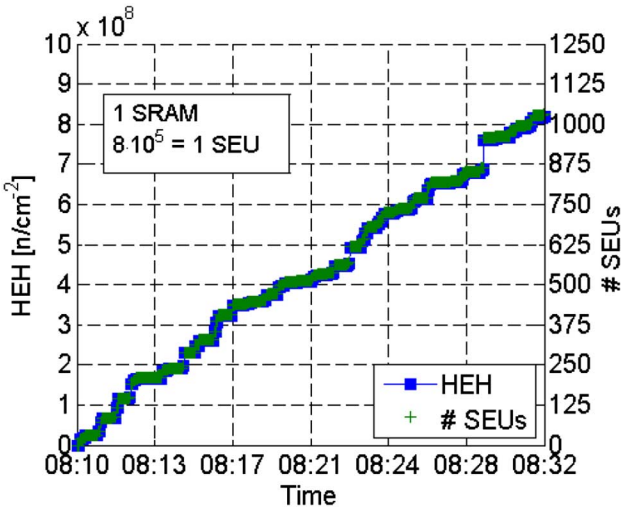

Fig. 6. Cypress SRAM measurements at a CERN mixed radiation facility with a flux of $7.5 \cdot 10^5$ cm^{-2}/s.

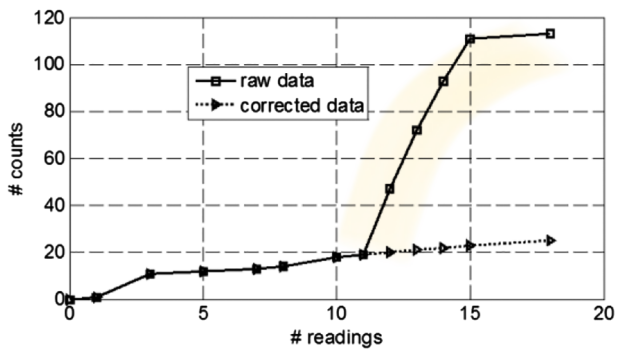

Fig. 7. Example of burst correction. Four consecutive bursts on three different SRAM blocks have been downscaled to 1 event.

an error burst can falsify the absolute measurement of the fluence. The investigation of this issue showed that the burst frequency increases when the chip is in read/write mode (related to the use of the pin Chip Select [10]), and happens in adjacent SRAM cells: several columns of the same IO in the same block are concerned. A countermeasure can be applied by reading the cells per block to recognize and correct burst error on-line, provided that the physical structure of the SRAM is known. The algorithm has been tried off-line on the data of the past campaigns and the results show that the total number of SEUs is reduced by a factor 5. The algorithm has been applied for runs of 30 s at two different fluxes of $1.7 \cdot 10^8$ cm^{-2}s^{-1} and $1 \cdot 10^7$ cm^{-2}s^{-1}. For the latter case, it has been possible to dump the SRAM memory during the irradiation each 5 s since the SEU rate is low and the comparison between the raw and the corrected data is shown in Fig. 7. Thus, the corrected cross section to be considered for the samples of the qualified lot is to be scaled by a factor 5 and would be $3.8 \cdot 10^{-14}$cm^2 which gives a resolution of $8 \cdot 10^5$ cm^{-2}/count and permits measuring with good statistics (> 100 counts) a fluence of $\sim 8 \cdot 10^7$ cm^{-2}. The sensitivity (HEH/count) satisfies the requirements described in Section II; although the accuracy is slightly lower than that foreseen this SRAM is employed in the new RadMon for the HEH flux measurements.

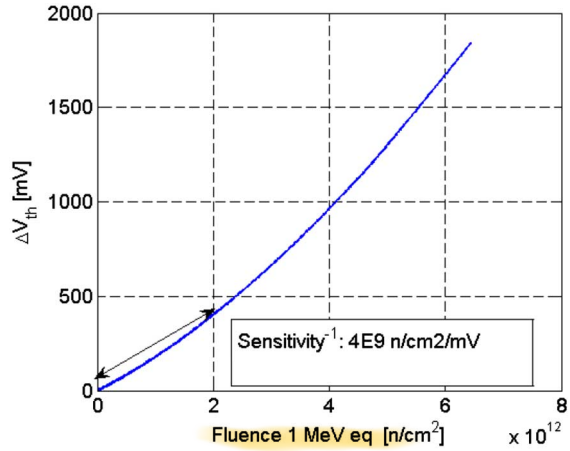

Fig. 8. Forward voltage variation of the series of three pin diodes as a function of 1 MeV neutron fluence.

C. Displacement Damage–Pin Diode

The Displacement Damage is quantified by means of the series of three p-i-n diodes BPW34FS from SIEMENS, pre-irradiated at 1 MeV neutron equivalent fluence of $4 \cdot 10^{12}$ n/cm^2, required to bring the sensor to a working point where it assures a sensitivity of 2.5 10^{-10} mV/n.cm^2($4 \cdot 10^9$ n/cm^2/mV). The reading circuitry injects a constant current to measure the forward voltage of the series of three diodes or one single diode. The three p-i-n diodes are used to have a higher resolution up to 10^{12} cm^{-2} (Fig. 8); moreover, the sensor board of the new RadMon can host another type of sensor, the LBSD diode, which can assure an even better resolution at low fluence ranges. The use of one SIEMENS p-i-n diode is for measuring high neutron fluences up to 10^{14} cm^{-2} with the Deported Module (Table V). To be able to read correctly the forward voltage of the diode a gain of 0.3 is applied to the analogue signal not to saturate the ADC input. Hence, this sensor and the measurement of the DD are extremely useful at high radiation levels (10^{14} cm^{-2}).

VI. Conclusion and Outlooks

We presented the new RadMon system which improved the radiation hardness by a factor 3 with respect to the previous version (from 8 krad(Si) to 25 krad(Si)). The TID limit is now imposed by the ADC. Several test campaigns with ^{60}Co sources, proton and neutron beams, and in a mixed fields were required to assure the radiation hardness of the electronics and characterize the sensors in order to improve the resolution of the monitor by a factor, ranging from 3 to 10, depending on the radiation damage considered (see summary Table V). The main data of the radiation test and calibration have been presented. The accuracy and the resolution of the TID measurements have been improved by using a more precise analogue circuitry and focusing the study on the 100 nm RadFET oxide which has been extensively characterized with both ^{60}Co and protons. The presented results can be achieved regardless the position of the sensors (Sensor Board or Deported Module). The possibility of applying a bias to the gate has been added. A new 400 nm has also been partially qualified with a ^{60}Co source to further improve the resolution. However more tests are required to quantify its accuracy

TABLE V
SENSOR PROPERTIES OF THE NEW RADMON (V6) COMPARED TO THE PREVIOUS VERSION (V5). * THE RESOLUTION FOR THE RADFET AND THE P-I-N DIODES IS EVALUATED IN THE RANGE 0-1KRAD, AND $0 - 2 \cdot 10^{11}$ n/cm^2, RESPECTIVELY. THE RESOLUTION FOR THE SRAM CORRESPONDS TO 100 COUNTS. THE VALUES FOR THE CYPRESS ARE OBTAINED WITH THE BURST CORRECTION

Sensor	Sensitivity^{-1}	Resolution		Range
		(V5)	(V6)	
Fet100	50 Rad/mV	300 rad	20 rad	1 Mrad
Fet100 Bias	14 rad/mV	NA	6 rad	0.4 Mrad
BPW (3)	$4{\cdot}10^9$ n/cm^2/mV	$3{\cdot}10^{10}$ n/cm^2	$6{\cdot}10^9$ n/cm^2	10^{13} n/cm^2
BPW (1)	$1{\cdot}10^{10}$ n/cm^2/mV	$7{\cdot}10^{10}$ n/cm^2	$2{\cdot}10^{10}$ n/cm^2	$5{\cdot}10^{14}$ n/cm^2
LBSD	$2{\cdot}10^8$ n/cm^2/mV	NA	$3{\cdot}10^8$ n/cm^2	$2{\cdot}10^{10}$ n/cm^2
Toshiba	$2{\cdot}10^6$ n/cm2/count	$2{\cdot}10^8$ n/cm^2	$2{\cdot}10^8$ n/cm^2	$2{\cdot}10^{11}$ n/cm^2
Cypress	$8{\cdot}10^5$ n/cm^2/count	NA	$8{\cdot}10^7$ n/cm^2	$4{\cdot}10^{11}$ n/cm^2

with charged particles. The hadron flux counter has also been improved by using larger and more sensitive SRAM. The use of two memory banks, populated with the TOSHIBA (sensitive to thermal neutrons) and CYPRESS (not sensitive to thermals) and the remote control of the voltage supplies permit to measure the HEH and the thermal neutron fluence without any intervention on the device. However, the use of the CYPRESS SRAM raised the issue of burst events which compromises the accuracy of the measurement. A correcting algorithm, which can be implemented on-line with the FPGA, has been applied to data of previous campaigns. The bursts are corrected but, as a consequence, the sensitivity decreases. For further improvements, the same SRAM with a larger size can be used or other types of SRAM are to be tested. The modularity of the RadMon architecture will permit a relative easy exchange of the SRAMs by only adopting the SensorBoard layout.

The obtained results, and the remote control and data taking of the RadMon triggered the interest of other research centres. RadMon prototypes have been used at the Centre Energie Atomique Valduc, the Jefferson Laboratory (JLAB), the Japan Proton Accelerator Research Center, and the Oak Ridge National Laboratory. The data presented in this paper for the two types of RadFETs highlights how the 100 nm RadFET can be used to replace thicker oxide RadFETs which exhibits many source of uncertainties, a result of interest for the space community.

To date the prototyping phase is completed and a production of one hundred units of the new RadMonV6 has been installed in the LHC injection lines and in the new CERN test facility. Finally, the monitor will be adapted to achieve the space requirements to make it fly on a cubeSat mission.

REFERENCES

[1] K. Roeed, M. Brugger, and G. Spiezia, "An overview of the radiation environment at the LHC in light of R2E irradiation test activities," in *CERN*, Geneve, CH, 2011 [Online]. Available: https://cds.cern.ch/record/1382083?ln=en, ATS-Note-2011-077 TECH

[2] R. Alia, B. Biskup, M. Brugger, M. Calviani, C. Poivey, K. Roeed, F. Saigne, G. Spiezia, and F. Wrobel, "SEU measurements and simulations in a mixed field environment," *IEEE Trans. Nucl. Sci.*, vol. 60, no. 4, pp. 2469–2476, Aug. 2013.

[3] G. Spiezia, J. Mekki, S. Batuca, M. Brugger, M. Calviani, A. Ferrari, D. Kramer, R. Losito, A. Masi, A. Nyul, P. Peronnard, C. Pignard, K. Roeed, and T. Wijnands, "The LHC accelerator radiation monitoring system," *J. Proc. Sci.* [Online]. Available: http://pos.sissa.it/archive/conferences/143/024/RD11_024.pdf

[4] "CHARM website," [Online]. Available: www.cern.ch/charm

[5] J. Mekki, M. Brugger, S. Danzeca, L. Dusseau, K. Roeed, and G. Spiezia, "Mixed particle field influence on radFET responses using co-60 calibration," *IEEE Trans. Nucl. Sci.*, vol. 60, no. 4, pp. 2435–2443, Aug. 2013.

[6] S. Metzger, S. Hoeffgen, T. Kuendgen, G. Spiezia, M. Brugger, S. Danzeca, J. Mekki, and P. Oser, "Study of parameters influencing the response of RadFETs," in *Proc. RADECS*. U.K.: Oxford, 2013.

[7] G. Spiezia, RADMON test–CEA CERN, Geneve, CH, report 1181667v1, 2011 [Online]. Available: https://edms.cern.ch/document/1181667/1

[8] D. Kramer, M. Brugger, V. Klupak, C. Pignard, K. Roeed, G. Spiezia, L. Viererbl, and T. Wijnands, "LHC RADMON SRAM detectors used at different voltages to determine the thermal neutron to high energy hadron fluence ratio," *IEEE Trans. Nucl. Sci.*, vol. 58, no. 3, pp. 1117–1122, Jun. 2011.

[9] K. Roeed, M. Brugger, D. Kramer, P. Peronnard, C. Pignard, G. Spiezia, and A. Thornron, "Method for measuring mixed field radiation levels relevant for SEEs at the LHC," *IEEE Trans. Nucl. Sci.*, vol. 59, no. 4, pp. 1040–1047, Feb. 2012.

[10] S. Danzeca, G. Spiezia, M. Brugger, L. Dusseau, G. Foucard, R. Garcia Alia, P. Mala, A. Masi, P. Peronnard, J. Soltes, A. Thornton, and L. Viererbl, "Qualification and characterization of SRAM memories used as radiation sensors in the LHC," in *presented at the Nuclear and Space Radiation Effects Conf.*. Paris, Fr: , 2014.

[11] J. O. Goldsten, R. H. Maurer, P. N. Peplowski, A. G. Holmes-Siedle, C. C. Herrmann, and B. H. Mauk, "The engineering radiation monitor for the radiation belt storm probes mission," *Space Sci. Rev.*, vol. 179, no. 1–4, pp. 485–502, 2013.

[12] A. Mohammadzadeh, H. Evans, P. Nieminen, E. Daly, P. Vuilleumier, P. Bühler, C. Eggel, W. Hajdas, N. Schlumpf, A. Zehnder, J. Schneider, and R. Fear, "The ESA standard radiation environment monitor program first results from PROBA-I and INTEGRAL," *IEEE Trans. Nucl. Sci.*, vol. 50, no. 6, pp. 2272–2277, Dec. 2003.

[13] G. Spiezia, M. Brugger, S. Danzeca, R. Garcia Alia, R. Gaillard, E. Fadakis, G. Foucard, R. Losito, A. Masi, J. Mekki, P. Oser, P. Peronnard, G. Ruggiero, and R. Secondo, "Compendium of radiation-induced effects for candidate particle accelerator electronics," in *Proc. Data Workshop Nucl. Space Rad. Effects Conf.*, San Francisco, CA, 2013.

[14] A. Masi, G. Spiezia, P. Peronnard, M. Donze, M. Brugger, and R. Losito, "The new generation of the CERN accelerator radiation monitoring system for electronics," *IEEE Trans. Nucl. Sci.*, vol. 60, no. 5, pp. 3475–3482, Oct. 2013.

[15] S. Danzeca, J. Cesari, M. Brugger, L. Dusseau, A. Masi, A. Pineda, and G. Spiezia, "Characterization and modelling of a floating gate dosimeter with gamma and protons at various energies," in *presented at the Nuclear and Space Radiation Effects Conf.*, Paris, Fr, 2014.

[16] A. Hands, P. Morris, C. Dyer, K. Ryden, and P. Truscott, "Single event effects in power MOSFETs and SRAMs due to 3 MeV, 4 MeV and fission neutrons," *IEEE Trans. Nucl. Sci.*, vol. 58, no. 3, pp. 952–959, Jun. 2011.

[17] G. Tsiligiannis, L. Dilillo, A. Bosio, P. Girard, S. Pravossoudovitch, A. Todri, A. Virazel, H. Puchner, C. Frost, F. Wrobel, and F. Saigné, "Multiple cell upset classification in commercial SRAMs," *IEEE Trans. Nucl. Sci.*, vol. 61, no. 4, pp. 1747–1754, Aug. 2014.